Int. J. Morphol.,
44(3):934-948, 2026.

The Anticancer Action of Bergenin in NNK-Induced Pulmonary Cancer: Mechanisms Involving nAChR/Src/STAT3 Activation of the Renin-Angiotensin System and IGF-1R Signaling

Acción Anticancerígena de la Bergenina en el Cáncer Pulmonar Inducido por NNK: Mecanismos que Involucran la Activación del Sistema Renina-Angiotensina por nAChR/Src/STAT3 y la Señalización del IGF-1R

Qing Cheng[1]; Ting Yang[2] & Conghua Chen[3]

CHENG, Q.; YANG, T. & CHEN, C. The anticancer action of Bergenin in NNK-induced pulmonary cancer: Mechanisms involving nAChR/Src/STAT3 activation of the renin-angiotensin system and IGF-1R signaling. *Int. J. Morphol., 44(3)*:934-948, 2026.

SUMMARY: The renin–angiotensin (RA) system has been linked to lung cancer development, yet detailed mechanistic insights remain limited. Bergenin, a traditional medicinal compound with demonstrated anti-tumor properties, was evaluated for its effects on non-small cell lung cancer (NSCLC) using a mouse xenograft model. Fifty athymic nude mice were allocated into five groups: a control group, an untreated NSCLC group, a doxorubicin (DOX)–treated group, a Bergenin-treated group, and a Bergenin plus DOX combination group. Bergenin was administered orally at 50 mg/kg/day, while DOX was delivered intraperitoneally at 50 mg/kg on days 10, 20, and 30. Tumor growth was tracked by measuring size, volume, and weight, and survival was analyzed with Kaplan–Meier estimates. Biochemical and histopathological assessments showed that Bergenin modulated oxidative stress markers, attenuated inflammatory mediators (IL-6, TNF-α, IL-8, Ang II, IFN-γ), and impeded tumor progression. The treatment downregulated signaling pathways associated with tumor cell survival, proliferation, and metastasis, including nAChR/Src/STAT3 and IGF-1R. Immunohistochemical analysis demonstrated reduced AGT expression, consistent with diminished tumor cell proliferation. Molecular investigations supported Bergenin's influence on critical apoptosis and angiogenesis pathways. In combination with DOX, Bergenin amplified therapeutic efficacy, indicating a potential synergistic interaction. Our results suggest that Bergenin may serve as a therapeutic agent targeting nAChR/Src/STAT3 and IGF-1R/Akt related signaling cascades in NSCLC, providing a promising complementary strategy to standard chemotherapy.

KEY WORDS: Bergenin; nAChR/Src/STAT3; Doxorubicin; Lung cancer; A549 cells.

INTRODUCTION

Lung cancer remains a leading cause of cancer mortality worldwide, with an estimated 2.2 million new cases reported in 2020 and an overall five-year survival around 19 %, driven largely by the dominant non-small cell lung cancer (NSCLC) subtype. NSCLC accounts for roughly 85 % of cases, while small cell lung cancer (SCLC) comprises about 15 % and tends to be more aggressive. Despite advances, therapeutic outcomes vary by stage, with localized NSCLC achieving roughly 60 % five-year survival and distant metastases dropping to about 6 % (Sung *et al*., 2021). The A549 cell line, derived from a 58-year-old male patient, serves as a widely used NSCLC model for mechanistic studies and preclinical evaluations of anti-tumor strategies (Islam *et al*., 2022). In this context, signaling networks centered on nicotinic acetylcholine receptors (nAChRs) and Src family kinases orchestrate oncogenic programs: a7-nAChR activation by nicotine can drive pro-proliferative pathways such as MAPK/ERK, PI3K/AKT, and, in certain settings, STAT3, while Src kinases act as hubs that propagate signals from nAChRs, EGFR, and IGF-1R to promote cell growth, invasion, and angiogenesis (Boo *et al*., 2023). STAT3, activated by JAKs and by Src, EGFR, and IGF-1R, upregulates anti-apoptotic and cell-cycle–driving genes (e.g., BCL-2 family members and Cyclin D1) and pro-angiogenic factors (VEGF), contributing to tumor progression and therapy resistance. IGF-1R signaling further amplifies these networks through IRS–PI3K–AKT and RAS–ERK axes, supporting metabolic adaptation and survival, with cross-talk among these pathways frequently strengthening oncogenic signaling, particularly in smoking-associated lung cancers (Salminen *et al*., 2021).

[1] Department of Respiratory and Critical Care Medicine, Wuhan Third Hospital, Tongren Hospital of WuHan University, Wuhan Hubei, China.
[2] Department of Pulmonary and Critical Care Medicine, Huai'an Hospital of Huai'an City (Huai'an Clinical Medical College of Jiangsu University Huai'an, Jiangsu, China.
[3] Department of Thoracic Surgery, Yangxin County People's Hospital, Huangshi, Hubei, China.
Qing Cheng and Ting Yang are co-first authors, they contributed equally to this work.

Received: 2026-04-29 Accepted: 2026-05-31

Collectively, co-activation of nAChR/Src/STAT3 and IGF-1R pathways fosters aggressive tumor phenotypes, therapeutic resistance, and epithelial-to-mesenchymal transition, underscoring these axes as compelling targets for combination therapies. Pharmacodynamic biomarkers such as phosphorylated SRC, STAT3, and IGF-1R, along with downstream effectors like Cyclin D1, VEGF, and MMPs, provide readouts of pathway engagement and treatment response (Nikzad *et al*., 2025). Multi-target strategies—pairing nAChR or Src inhibition with STAT3 or IGF-1R blockade—hold promise for overcoming compensatory signaling and achieving synergistic anti-tumor effects, particularly when patient selection is guided by molecular signatures of these pathways to optimize NSCLC outcomes. Clinically, patients contend with substantial morbidity from disease and treatment-related toxicities, and standard regimens often combine platinum-based agents with taxanes or gemcitabine, while anthracyclines like doxorubicin (DOX) remain integral in many regimens, sometimes in combination with adjuncts that enhance efficacy and mitigate adverse effects (Dai *et al*., 2025).

Bergenin, a bioactive benzopyran glycoside derived from plants such as *Belamcanda chinensis* and *Gaertnera vaginata*, has emerged as a multi-targeted anti-cancer agent with anti-inflammatory, antioxidant, and immunomodulatory properties. Across preclinical models, Bergenin inhibits proliferation, promotes apoptosis, and suppresses metastasis and angiogenesis, potentially by dampening oxidative stress and inflammatory signaling and by modulating key oncogenic pathways (Pandey *et al*., 2025). Mechanistically, Bergenin can downregulate NF-κB–driven inflammatory mediators, reduce pro-survival and pro-angiogenic factors like VEGF, and influence apoptotic regulators such as BCL-2 family proteins; in lung cancer models, it has been linked to reduced cell growth, cell-cycle arrest, and enhanced chemosensitivity (Ju Hwang *et al*., 2019). Pharmacokinetic data remain limited and largely preclinical, with ongoing efforts to improve bioavailability and delivery. Given its broad target spectrum and relative safety in traditional use, Bergenin is being explored as a complementary agent in cancer therapy, including NSCLC, where it may synergize with conventional chemotherapies or targeted therapies by attenuating tumor-promoting inflammation, oxidative stress, and survival signaling (Kumar *et al*., 2025). Robust in vivo validation, mechanism-focused studies, and well-designed clinical trials are needed to define its therapeutic potential, optimal formulations, and safety profile in humans. This study explores whether combining Bergenin with doxorubicin can suppress A549 lung cancer cells in athymic nude mice by targeting the nAChR/Src/STAT3 axis, Renin–Angiotensin System activation, and IGF-1R signaling pathway.

MATERIAL AND METHOD

Study design

A549 and human umbilical vein endothelial (HUVEC) cells were cultured in DMEM supplemented with 10% fetal bovine serum and maintained at 37 °C in a 5 % CO_2 atmosphere. When the cell monolayer reached more than 85 % confluence, passaging was performed using 0.25 % trypsin to detach the cells for subculture.

All animal experiments were approved by the Ethics Committee of Wuhan Third Hospital and conducted in accordance with the National Institutes of Health guidelines for the care and use of laboratory animals. Six-week-old male athymic nude mice, sourced from Wuhan Third Hospital, Tongren Hospital of WuHan University, Wuhan Hubei, China were used. The animals were kept in a temperature- and humidity-controlled facility on a 12-hour light/12-hour dark cycle with *ad libitum* access to food and water.

Following a two-week acclimation, each mouse received a subcutaneous injection of 1×10^6 A549 cells suspended in a 1:1 mixture with Matrigel (Biomatrix/ Biosciences, San Jose, CA, USA) into the right flank to establish xenografts.

Five days post-implantation, forty tumor-bearing mice were randomly assigned (n = 10 per group) alongside ten tumor-free BALB/c nude controls and observed for 40 days. The experimental groups were: (i) Sham, non-tumor-bearing mice receiving daily gavage with 50 μL saline; (ii) A549, tumor-bearing mice without treatment; (iii) DOX, tumor-bearing mice receiving 50 mg/kg doxorubicin intraperitoneally on days 10, 20, and 30; (iv) Bergenin, tumor-bearing mice given 50 mg/kg/day Bergenin by gavage; and (v) Bergenin + DOX, tumor-bearing mice treated with 50 mg/kg DOX intraperitoneally on days 10, 20, and 30 and 50 mg/kg/day Bergenin by gavage (Ekinci Akdemir *et al*., 2025; Ma *et al*., 2022).

Tumor size measurement

Tumor growth was monitored weekly by calculating volume with the formula:

$$\text{Volume } (mm^3) = [(\text{width})^2 \times \text{length}] / 2.$$

Survival outcomes were analyzed using the Kaplan-Meier method. At study end or when humane endpoints were reached, mice were anesthetized and euthanized with ketamine (10 % solution, 15 mg/kg, intraperitoneally) and

xylazine (2 % solution, 80 mg/kg, intraperitoneally). Tissues and samples were collected for downstream analyses (Akbaribazm *et al*., 2020).

Serum cytokine and Ang II levels

Four sterile 500 µL vials were prepared, each containing 200 µL of dilution buffer and labeled as standard numbers 1 through 4. To generate standard number 5, 650 µL of dilution buffer was added to the parent standard (CN: KPG-MI6S) and incubated for 15 min at room temperature, yielding a concentration of 500 pg/mL. Subsequently, 100 µL from standard 5 was transferred into standard 4, mixed, and incubated for 3 min; this dilution step was repeated sequentially down to standard 1, producing concentrations of 6.166 pg/mL (standard 4), 5.55 pg/mL (standard 3), 5.18 pg/mL (standard 2), and 6.1 pg/mL (standard 1).

For the assay, 50 µL of diluted primary antibodies targeting IL-6, Ang II, IL-8, IFN-γ, and TNF-α (BioLegend, USA) were added to each well of a 96-well microplate, which were then covered and incubated with gentle shaking at 300 rpm overnight. The wells were washed three times with the washing solution (KPG-WB), after which 300 µL of blocking solution (FBS) was added and incubated for an additional hour with shaking. After another wash, 50 µL of standards or samples (diluted as needed) and a control dilution were added to each well and incubated with shaking for 2 hours.

Following a further wash, 50 µL of the diluted secondary antibody–HRP–Avidin complex (KPG-HA) was added, the plate covered, and incubated for 2 hours with shaking. After washing again, 50 µL of diluted enzyme (KPG-EB) was added, covered, and incubated for 20 min. The wells were washed once more before adding 50 µL of dye solution (TMB) and allowing color development in the dark for 15 min. The reaction was halted by adding 25 µL of stopping solution (KPG-ST), and absorbance was read at 450 nm with an ELISA reader. Standard absorbance values were used to construct a standard curve, enabling concentration calculations for samples; all measurements were conducted in duplicate for standards, samples, and controls, and averaged (Pearl *et al*., 2018).

Serum SOD, CAT, and GPx activity

CAT assay

Serum catalase (CAT) activity was determined using another commercial ELISA kit (ab100764, Abcam, Michigan, USA) based on a colorimetric reaction of excess H2O2 with a chromogen. In a 96-well plate, 100 µL of 100 mM potassium phosphate buffer and 20 µL of 0.1 M H2O2 were mixed, then 20 µL of serum was added. After a 20-minute incubation in the dark, 30 µL of Purpald (chromogen) and 30 µL of 40 mM KOH were added, followed by a second 20-minute dark incubation. Finally, 2 µL of catalase potassium periodate was added and incubated for 20 min. Absorbance was read at 540 nm using a spectrophotometer, with results reported in U/mL, including standards and blanks (Tekin & Seven, 2022).

SOD assay

Serum superoxide dismutase (SOD) activity was quantified using a commercial ELISA kit (E-EL-R1424, Elabscience, Cambridge, MA, USA) per the manufacturer's protocol, with detection on a microplate reader. Each well received 200 µL of WST SOD buffer and 20 µL of working enzyme, followed by 100 µL of serum sample. After 37 °C incubation for 20 min, absorbance was measured at 450 nm on a spectrophotometer (Shimadzu UV-1800, Japan) and reported in U/mL (Tekin & Seven, 2022).

GPx assay

GPx activity in serum was measured with the Randox ELISA kit (Cat. No. RS504). The assay follows the GPx-catalyzed oxidation of GSH to GSSG, with GSSG subsequently reduced back to GSH by glutathione reductase (GR) using NADPH, whose conversion to NADP+ is monitored by absorbance at 340 nm. Serum samples were prepared by diluting 50 µL of serum with 100 µL of buffer, then centrifuging and transferring the supernatant to a 96-well plate containing buffers, substrates, and NADPH. Background and positive controls were included. After adding Cumene Hydroperoxide, absorbance was read at two time points, and ΔA340/min was calculated as |A340(Time 2) - A340(Time 1)|/(Time 2 - Time 1). GPx activity was derived as: $|\Delta A340|/\text{min} \div 0.0037 \times 8.5 \times 0.5 \times$ sample dilution. Results were reported in U/mL (Tekin & Seven, 2022).

Serum nitric oxide (NO) levels

NO levels were not measured directly due to the instability of nitric oxide. Instead, nitrite and nitrate concentrations in various fluids were used as surrogate indicators of NO production. In the assay, 400 µL of serum was deproteinized by adding 6 mg of zinc sulfate, followed by centrifugation at 12,000 × g for 15 min. From the supernatant, 100 µL were mixed with 100 µL of vanadium (III) chloride solution and the Griess reagent (consisting of sulfanilamide and N-(1-naphthyl) ethylenediamine

dihydrochloride) and incubated at 37°C for 30 min. Absorbance was read at 450 and 630 nm, and nitrite/nitrate concentrations were determined by interpolation on a standard curve prepared with sodium nitrate ranging from 0 to 200 μM (Mohana *et al*., 2023).

Tumor tissue thiobarbituric acid reactive substances (TBARS), thiol, and ferric reducing antioxidant power (FRAP) levels

This assay relies on tissue capacity to reduce Fe(III) to Fe(II) in the presence of the Fe(III)-TPTZ complex (FRAP reagent). To perform the assay, 50 μL of FRAP working solution was combined with 200 μL of homogenized tumor tissue and incubated for 4 min at 37 °C. Antioxidants in the sample reduce the Fe(III)-TPTZ complex to the blue Fe(II)-TPTZ product, detectable at 593 nm. After incubation, the mixture was centrifuged for 10 min at 15,000 × *g*, and the absorbance of the supernatant was measured against a blank at 593 nm. A standard curve was generated using $FeSO_4$ standards ranging from 0 to 1000 μM, enabling calculation of the sample ferric reducing antioxidant power (FRAP) values.

Lipid peroxidation in tumor tissue was assessed using the TBARS assay. A 100 μL homogenate was mixed with 50 μL thiobarbituric acid, 2 μL butylated hydroxytoluene (BHT), and 50 μL phosphoric acid, then incubated at 37 °C for 30 min. The reaction mixture's absorbance was measured at 532 nm with a Stat Fax ELISA reader. TBARS concentrations were expressed as nmol malondialdehyde (MDA) per mg protein.

For thiol quantification, a 50 mg homogenate was diluted with 250 μL of Tris-EDTA and incubated at 25 °C for 10 min. The initial absorbance (A) was read at 412 nm (a) using a Stat Fax ELISA reader. Then, 20 μL of DTNB (Ellman's reagent) was added, and the mixture incubated for an additional 20 min at 25 °C. The final absorbance (b) was recorded at 412 nm, and the absorbance of the DTNB blank (μ) was measured as well. The total thiol concentration was calculated as:

Total thiol (μM) = (β - α - μ) × 1.07 / 6.8 (Cuellar-Rufino *et al*., 2022).

Real-time PCR

RNA Extraction

Total RNA was extracted with the GeneMATRIX Universal RNA Purification Kit (EURx Sp. z o.o, Cat. No. E3598-02, Poland). Tumor tissue (20 mg) and lung tissue (10 mg) were finely ground. RNA was isolated after removing genomic DNA using a homogenization spin-column, followed by RNA binding and elution with an RNA-binding spin-column according to the kit protocol (Faraji *et al*., 2025).

cDNA Synthesis

After confirming the integrity of the total RNA, 1 μg of RNA was reverse-transcribed into complementary DNA (cDNA) using the PrimeScript™ RT Reagent Kit (Perfect Real Time) from Takara Bio Inc. (Japan, Cat. No. RR037A). The cDNA synthesis was prepared on ice in a 10 μL reaction volume containing 2 μL PrimeScript buffer, 0.5 μL each of Random Hexamers (100 μM) and Oligo(dT) (50 μM), 0.5 μL PrimeScript RT Enzyme Mix, and 1 mg total RNA, with RNase-free distilled water added to reach 10 mL. The mixture was incubated at 37 °C for 15 min and then heat-inactivated briefly at 85 °C for 5 s.

Quantitative real-time PCR was performed using TB Green® Premix Ex Taq™ (Takara Bio Inc., Japan, Cat. No. RR420A). For the qPCR setup on the Applied Biosystems StepOne Real-Time PCR System, the reaction consisted of 10 μL TB Green Premix Ex Taq, 0.4 μL of each primer, 0.4 μL ROX Reference Dye, and 1 μL template in a final volume of 20 μL, brought to volume with sterile purified water. GAPDH served as the housekeeping gene, and gene expression was analyzed using the $2^{-\Delta\Delta CT}$ method.

Primers for the target genes were designed with AlleleID software (v7.5, Premier Biosoft, USA) and validated with NCBI Primer-BLAST (https://www.ncbi.nlm.nih.gov/tools/primer-blast/). The expression levels of Src, nAChR, STAT3, Akt, AGT, and IGF-1R were measured to evaluate tumor cell proliferation, angiogenesis, survival, and differentiation. The primer sequences used in this study are provided in Table I.

Table I. Primer sequences.

Gene	Sequences (5`–3`)
GAPDH	Forward: AGGTCGGAGTCAACGGATTTG
	Reverse: TGCCCAGGATGCCCTTCTCC
AGT	Forward: ATGGAAGGAGGCTGAGGTTG
	Reverse: TCAGGAGGAGGAGGAGGTTG
IGF-1R	Forward: ATGGCTGCTGCTGAGGACAA
	Reverse: TCACTGCTCAGGCTTCTGGT
Src	Forward: ATGGCAGCAGCAGCAGGTTG
	Reverse: TCACTGCTCAGGCTGCTGGT
nAChR	Forward: ATGGTGCTGCTGCTGCTGTT
	Reverse: TCACTGCTCAGGCTGCTGGT
STAT3	Forward: ATGGCTGCTGCTGCTGCTGTT
	Reverse: TCACTGCTCAGGCTGCTGGT
Akt	Forward: ATGGCTGCTGCTGCTGCTGTT
	Reverse: TCACTGCTCAGGCTGCTGGT

$\Delta\Delta Ct = [(Ct_{Target}\text{-}Ct\ GAPDH)_{test\ sample} - (Ct_{Target}\text{-}Ct\ GAPDH)_{control\ sample}]$.

The fold change (Gene expression) = $2^{-\Delta\Delta Ct}$ (Horiguchi *et al*., 2024).

Immunohistochemical assay

To conduct immunohistochemical (IHC) staining for AGT and STAT3 proteins, tumor tissues from mice were fixed in 10 % buffered formalin for 24 h at room temperature, then rinsed with phosphate-buffered saline (PBS). The samples were dehydrated in a graded ethanol series (70 %, 95 %, 100 %), cleared with xylene, and embedded in paraffin until solid. Sections 3–4 μm thick were sliced from the paraffin blocks using an RM2125 RTS microtome (Leica, USA) and mounted on glass slides to dry. Sections were deparaffinized in 100 % xylene (two changes, 5–10 min each) and rehydrated through 100 %, 95 %, 70 % ethanol, and finally PBS. Heat-induced epitope retrieval (HIER) was performed by boiling in citrate buffer (pH 6.0). All sections were blocked with 5 % bovine serum albumin for 30 min at room temperature to reduce nonspecific binding. Primary antibodies against AGT (cat. no. 23972-1-AP, 1:500, Proteintech) were diluted in Tris-buffered saline (TBS) and applied to the sections, which were incubated overnight at 4 °C or for 1 h at room temperature. After washing with PBS (three times, 5 min each) to remove unbound primary antibodies, a biotinylated rabbit anti-mouse IgG secondary antibody (BioLegend) diluted in 5 % BSA was added, followed by streptavidin–horseradish peroxidase, and incubation for 30 min at room temperature. Slides were washed again with PBS (three times, 5 min each) to remove excess secondary antibody. Visualization was performed with 1,3-diaminobenzidine (DAB) tetrahydrochloride, and sections were counterstained with hematoxylin. Stained slides were examined with a Cytation 5 Cell Imaging Multi-Mode Reader (BioTek). Positive cells were counted in 10 random fields of view per slide, and results were expressed as the mean percentage of AGT-positive cells (Patel *et al*., 2022).

Histopathological analysis of tumor and lung tissue

Histopathological evaluation of lung tissues was conducted using an optical microscope (model No. BX61TRF; Olympus, Japan) connected to ImageJ software. As with the IHC assay, 5 μm sections were mounted on slides and stained with hematoxylin to assess lung histology. Hematoxylin and eosin staining, a routinely used technique in histopathology, helps visualize cell nuclei, cytoplasm, and the extracellular matrix for lung tissue (Vasilescu *et al*., 2023).

Tissue preparation and stereological measurements

The lung tissue's primary volumes were determined using immersion techniques. After estimating the extent of tissue shrinkage, isotropic uniform random (IUR) sections were generated via the orientator method. Following processing, paraffin blocks were produced, 5-μm sections were sliced from the blocks (Leica Microsystems), and the sections were stained with hematoxylin and eosin (H&E).

For shrinkage calculation, the diameter of the circular section after processing was measured and used in the subsequent formula:

$$\text{Volume shrinkage} = 1 - (AA/AB)^{1.5}$$

$$A_0 = \pi D02/4$$

$$A_f = \pi Df2/4$$

$$\text{Area shrinkage factor} = \frac{A_f}{A_0} = \left(\frac{D_f}{D_0}\right)^2$$

$$\%\ \text{Area shrinkage} = \left(1 - \left(\frac{D_f}{D_0}\right)^2\right) \times 100\ \%$$

In 5-μm-thick sections, the volume densities of the targeted structures—lung volume (LV), tissue parenchyma volume (TPV), air parenchyma volume (APV), and vessels volume (VV)—were determined using the point-counting method and Delesse's formula.

$$Vv(structure) = \sum_{i=1}^{n} p\ (structure) / \sum_{i=1}^{n} (reference)$$

"$\sum_{i=1}^{n} p\ (structure)$" was the number of test points that settled on the targeted structures, and "$\sum_{i=1}^{n} p\ (structure)$" was the total number of points that fell on the lung sections. The following formula was used to determine the total targeted structural volume (Fig. 1) (Vasilescu *et al*., 2023).

$$V(structure) = V(total\ lung) \times Vv)structure)$$

Western blotting assay

After PBS washing and removal of debris and surrounding tissue, tumor cells were lysed at 4 °C using a lysis buffer containing protease inhibitors. The lysate was clarified by centrifugation at 15,000 *g* for 15 min at 4 °C, and protein concentration was determined with the BCA assay kit (Catalog No. 71285-3; Beyotime Institute of Biotechnology, China). A total of 20 μg of protein was loaded per lane on a 10 % SDS–PAGE gel and then transferred to a PVDF membrane (Millipore, Billerica, MA, USA). The membrane was

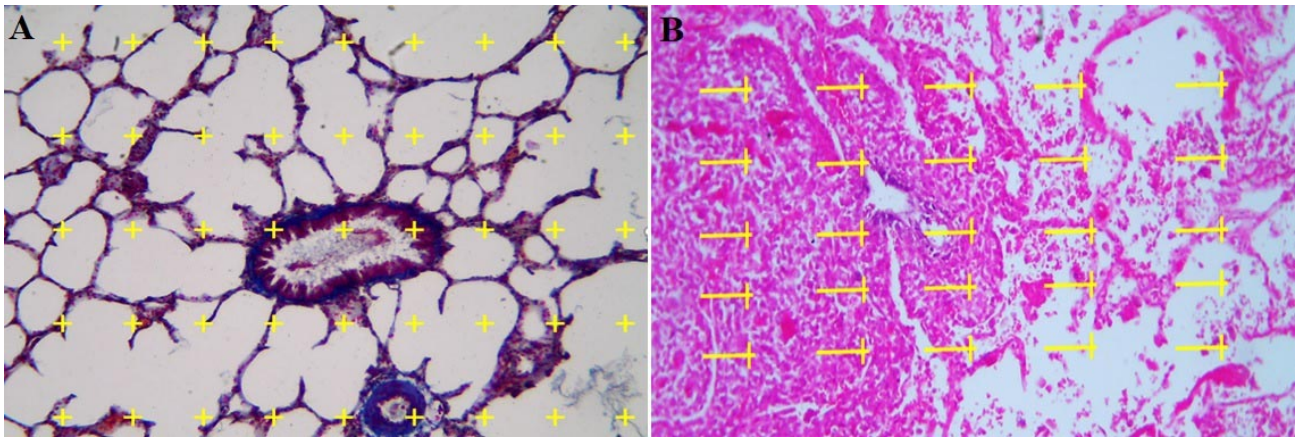

Fig. 1. (a) Point probe (25 points) and (b) Line probe (25 lines) are utilized to estimate the volume density of all structures. The total number of points (∑p) and lines within each structure, as well as the length of each line in the probe represented by linear magnification (l/p), are provided. Additionally, the number of lines situated within the internal regions of the structures (Σl) is noted. Finally, use these counts to compute the density at this level: $Sv = 2\times \Sigma l / \Sigma p \times l/p$ (H&E staining, ×40). Light photomicrograph of the lung.

incubated overnight at 4 °C with primary antibodies: anti-STAT3 (cat. no. 10025-2-AP; 1:500; Proteintech), anti-Src (cat. no. 51116-1-AP; 1:1000; Proteintech), anti-AGT (cat. no. 23972-1-AP; 1:500; Proteintech), and anti-β-actin (cat. no. ab8227; 1:400; Abcam). Blocking was performed using 5 % bovine serum albumin (BSA) and 0.1 % Tween-20 in TBST at 37 °C for 2 h. Following washes in PBS containing 0.1 % Tween-20, membranes were probed with HRP-conjugated goat anti-rabbit IgG (incubated at 25 °C for 2 h). Detection was carried out with the Servicebio chemiluminescence kit (Catalog No. G2020; Servicebio, Wuhan, China). Images were captured using a Bio-Rad ChemiDoc system and analyzed with ImageJ (Wu *et al*., 2019).

Statistical Analysis

Normality of the data was assessed with the Shapiro-Wilk test, and homogeneity of variances was evaluated using Levene's test ($p > 0.05$). Results are presented as mean ± SEM, with all experiments performed in triplicate. A one-way ANOVA was used to compare group means, followed by Dunnett's t post hoc test (two-tailed). Statistical analyses were conducted in SPSS software (Version 21; SPSS Inc., Chicago, IL), with significance set at $p < 0.05$. Survival analyses were carried out using the Kaplan-Meier method in GraphPad Prism (GraphPad Software, Boston, MA, USA, version 8.0.2).

RESULTS

Effects of bergenin on survival rate, body weight, and tumor volume

Mice were assessed on days 5, 10, 15, 20, 25, 30, 35, and 45 for body weight, tumor volume, and survival. Compared with Sham controls, the Bergenin-treated groups showed notable trends in body weight trajectories, with the following observations: the Bergenin+A549 and Bergenin+DOX+A549 groups exhibited greater weight gain than the A549 alone and DOX+A549 groups. Statistical analysis revealed a significant difference in body weight between Sham and A549 groups ($p<0.05$), and between Bergenin-treated groups and the A549 group ($p<0.05$). A more pronounced difference was observed between the Bergenin+ DOX+A549 group and the A549 group ($p < 0.05$) (Fig. 2a).

Post-induction, tumor volumes decreased significantly in the Bergenin-treated groups (Bergenin+A549 and Bergenin+DOX+A549) and in the DOX+A549 group relative to the A549 group ($p<0.05$ for comparisons where applicable) (Fig. 1B). Tumor volume trends over time are depicted in Figure 2B, with the DOX+A549 and Bergenin+ DOX+A549 groups showing the most pronounced reductions (Fig. 2b).

Survival curves indicated that the Bergenin-treated groups (Bergenin+A549 and Bergenin+DOX+A549) tended to display higher survival probabilities compared with the A549 and DOX+A549 groups. At the final time point, survival rates were highest in the Bergenin+DOX+A549 group, followed by Bergenin+A549, with Sham and DOX+A549 showing comparatively lower survival (Fig. 2c).

Effects of Bergenin on serum IL-6, IL-8, Ang II, IFN-γ, IL-1β, and TNF-α

Mean serum levels of IL-6, IL-8, Ang II, IFN-γ, IL-1β, and TNF-α were measured in the experimental groups (pg/dL). Compared with the Sham controls, the A549-containing groups showed significant alterations in several cytokines. Specifically, IL-6, IL-1β, Ang II, TNF-α, and IL-

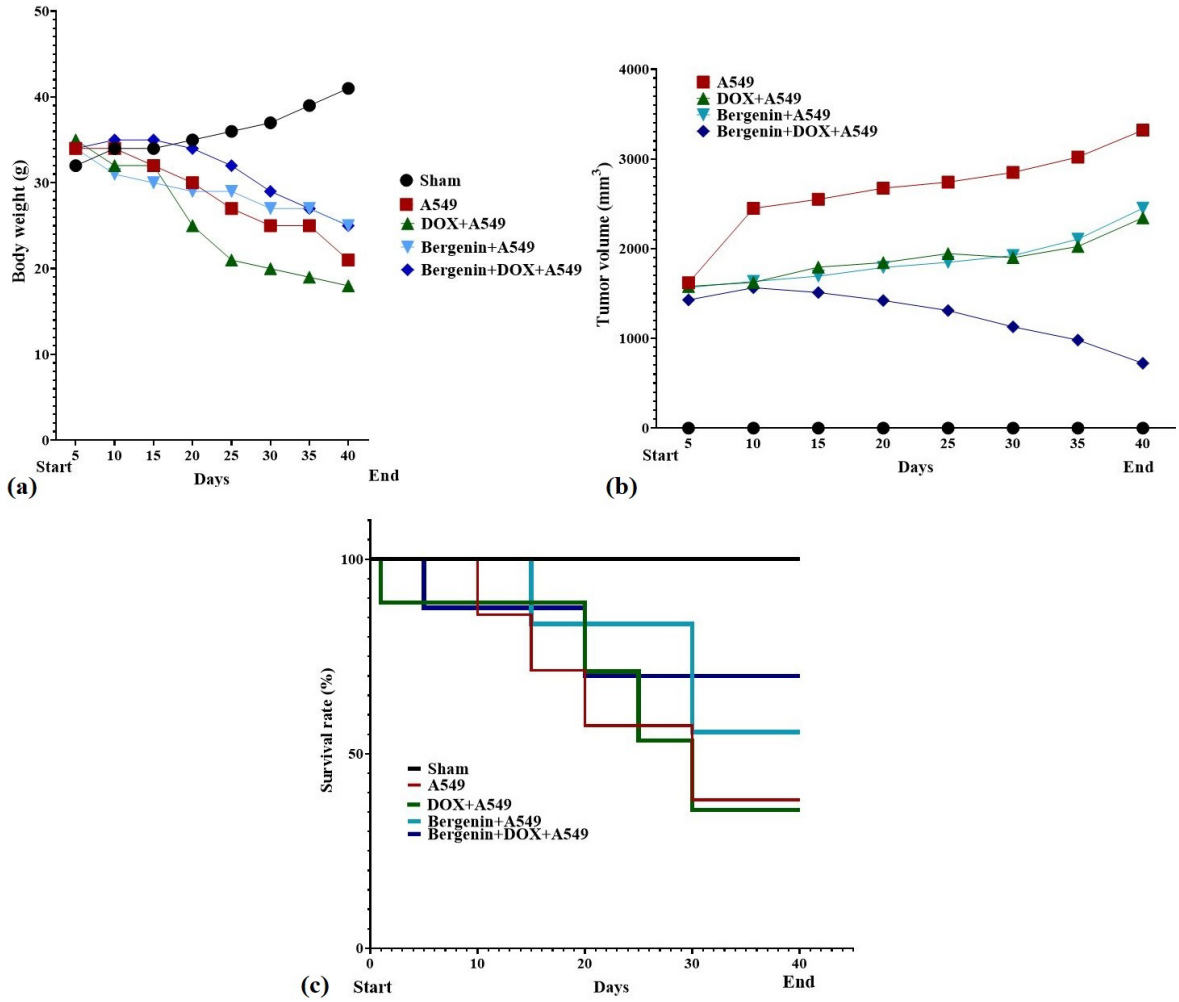

Fig. 2. (a) Body weight (g) over time; (b) Tumor volume (cm^3) over time; (c) Survival rate (%). Data are presented as means ± SD (n = 10 per group). Statistical annotations: [a] ($p < 0.05$) Sham *vs.* A549; [b] ($p < 0.05$) Bergenin-treated groups *vs.* A549; [c] ($p < 0.05$) Bergenin+DOX+A549 *vs.* A549.

8 levels differed across groups, while IFN-γ showed a distinct pattern of change. DOX treatment in the A549+DOX groups tended to elevate IL-6, IL-8, IL-1β, and TNF-α and reduce IFN-γ, although not all of these changes reached statistical significance versus A549 alone. In contrast, Bergenin-containing regimens (Bergenin+A549 and Bergenin+ DOX+A549) produced reductions in IL-6, IL-8, IL-1β, and TNF-α relative to A549 and A549+DOX groups, with varying levels of significance depending on the comparison ($p<0.05$ where indicated) (Fig. 3a).

Effects of Bergenin on serum SOD, GPx, CAT, and NO

Serum antioxidant enzymes and NO levels following bergenin-based treatment. Mean NO levels and serum activities of SOD, CAT, and GPx were measured across experimental groups. Compared with Sham controls, the A549-containing groups showed substantial alterations in NO and antioxidant enzyme activities. Specifically, NO levels were markedly elevated in the A549 group and persisted across subsequent treatments, with Bergenin-containing regimens showing a tendency toward NO reduction compared with A549 and DOX+A549 groups ($p < 0.05$ where indicated). SOD activity was reduced in the A549 group relative to Sham and partially restored by Bergenin-containing treatments; DOX+A549 alone did not produce a consistent improvement. Catalase (CAT) and glutathione peroxidase (GPx) activities followed a similar pattern, with A549 reducing CAT and GPx activities compared with Sham, and Bergenin-containing regimens (Bergenin+A549 and Bergenin+DOX+A549) showing significant increases relative to A549 ($p<0.05$). Overall, Bergenin treatment, alone or with DOX, mitigated oxidative stress markers compared with A549 alone (Fig. 3b).

Effects of Bergenin on tumor tissue FRAP, TBARS, and thiol

Tumor tissue oxidative stress and antioxidant capacity following Bergenin-based treatment. Mean tissue levels of total thiol, FRAP (μmol/mg protein), and TBARS (nmol/mg protein) were measured across experimental groups. Relative to Sham controls, the A549-containing groups showed alterations in all three markers. Specifically, thiol content tended to be reduced in the A549 group and waspartially restored by Bergenin-containing regimens (Bergenin+A549 and Bergenin+DOX+A549). FRAP values were markedly decreased in the A549 group compared with Sham, with Bergenin-containing treatments significantly increasing FRAP relative to A549 ($p<0.05$). TBARS levels were elevated in the A549 group, indicating increased lipid peroxidation, and were reduced by Bergenin-containing regimens, with significant differences versus A549 observed in the Bergenin-treated groups ($p<0.05$). Collectively, Bergenin alone or in combination with DOX mitigated oxidative stress in tumor tissue compared with A549 alone (Fig. 3c).

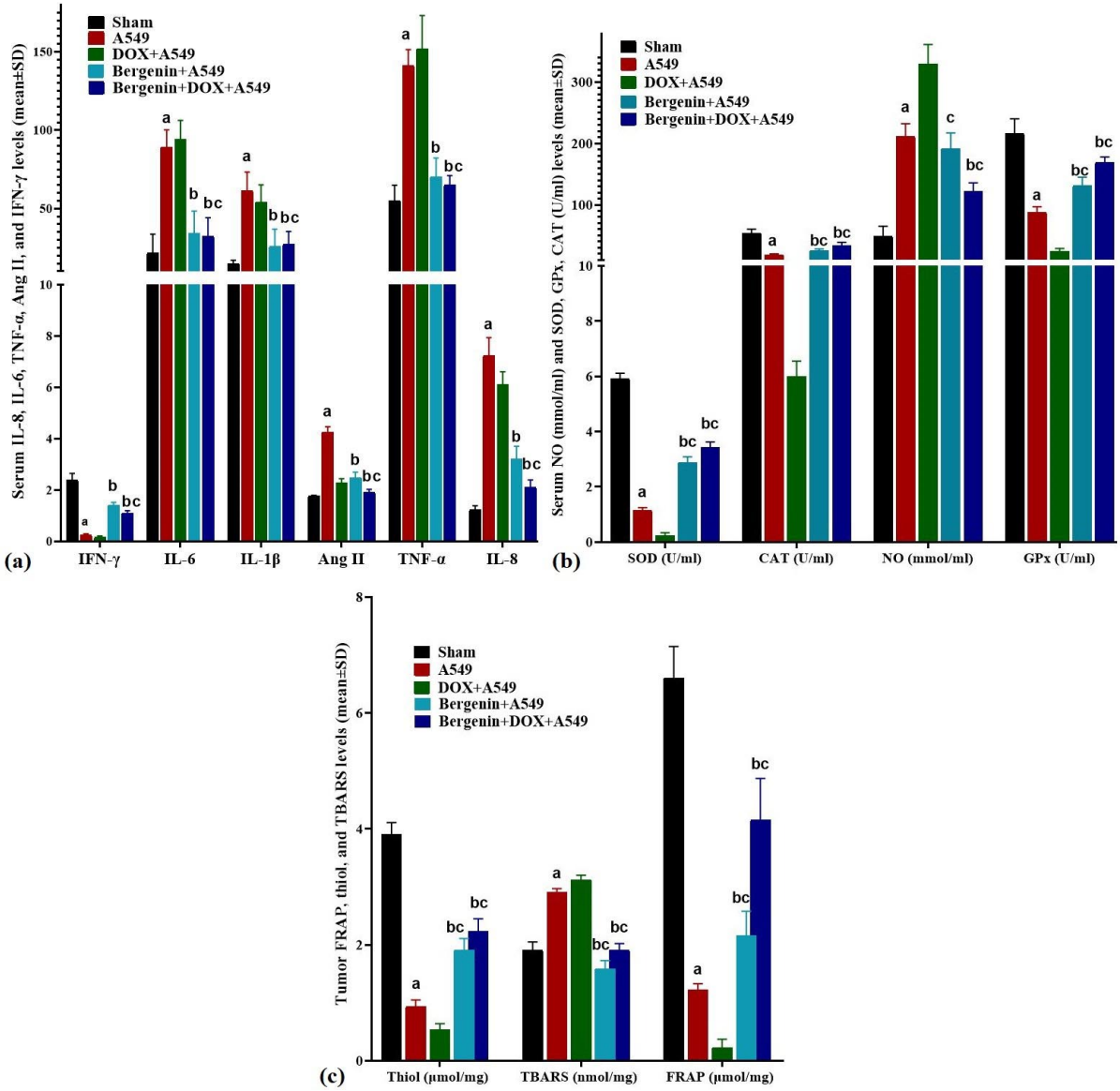

Fig. 3. (a) The mean mice serum levels of IL-6, IL-8, Ang II, IFN-γ, IL-1β, and TNF-α (pg/dl); (b) Mean NO levels (mmol/mL) and antioxidant enzyme activities (SOD, GPx, CAT in U/mL); (c) The mean mice tissue levels of total thiol, FRAP (μmol/mg protein) and TBARS (nmol/mg proteins) in experimental groups. Statistical annotations: [a]($p<0.05$) Sham *vs.* A549; [b]($p < 0.05$) Bergenin-treated groups *vs.* A549; [c]($p < 0.05$) Bergenin+DOX+A549 *vs.* A549.

Effects of Bergenin on tumor tissue AGT, IGF-1R, Src, nAChR, STAT3, and Akt genes expression

Expression of tumor tissue genes AGT, IGF-1R, Src, nAChR, STAT3, and Akt. The expression levels of AGT, IGF-1R, Src, nAChR, STAT3, and Akt in tumor tissue were measured across experimental groups. Compared with Sham controls, the A549 group showed marked upregulation in all six genes. Bergenin-containing treatments (Bergenin+A549 and Bergenin+DOX+A549) generally reduced gene expression relative to A549, with the Bergenin+DOX+A549 combination yielding the greatest declines for several targets. Across the panel, the Bergenin-treated groups demonstrated statistically significant decreases ($p<0.05$) versus the A549 group for multiple genes, while the Bergenin+DOX+A549 group often showed the strongest suppression. Details by gene are summarized below with the indicated significance markers (Fig. 4a).

Effects of Bergenin on tumor tissue AGT, Src, and STAT3 proteins expression

Expression of tumor tissue proteins AGT, Src, and STAT3 (normalized to β-actin). The protein levels of Src/b-actin, AGT/b-actin, and STAT3/β-actin were measured in tumor tissue across experimental groups. Relative to Sham controls, the A549 group showed alterations in all three targets. Bergenin-containing regimens (Bergenin+A549 and Bergenin+DOX+A549) generally reduced the expression of these proteins compared with A549 alone, with the Bergenin+DOX+A549 combination often yielding the greatest suppression (Fig. 4b, 4c).

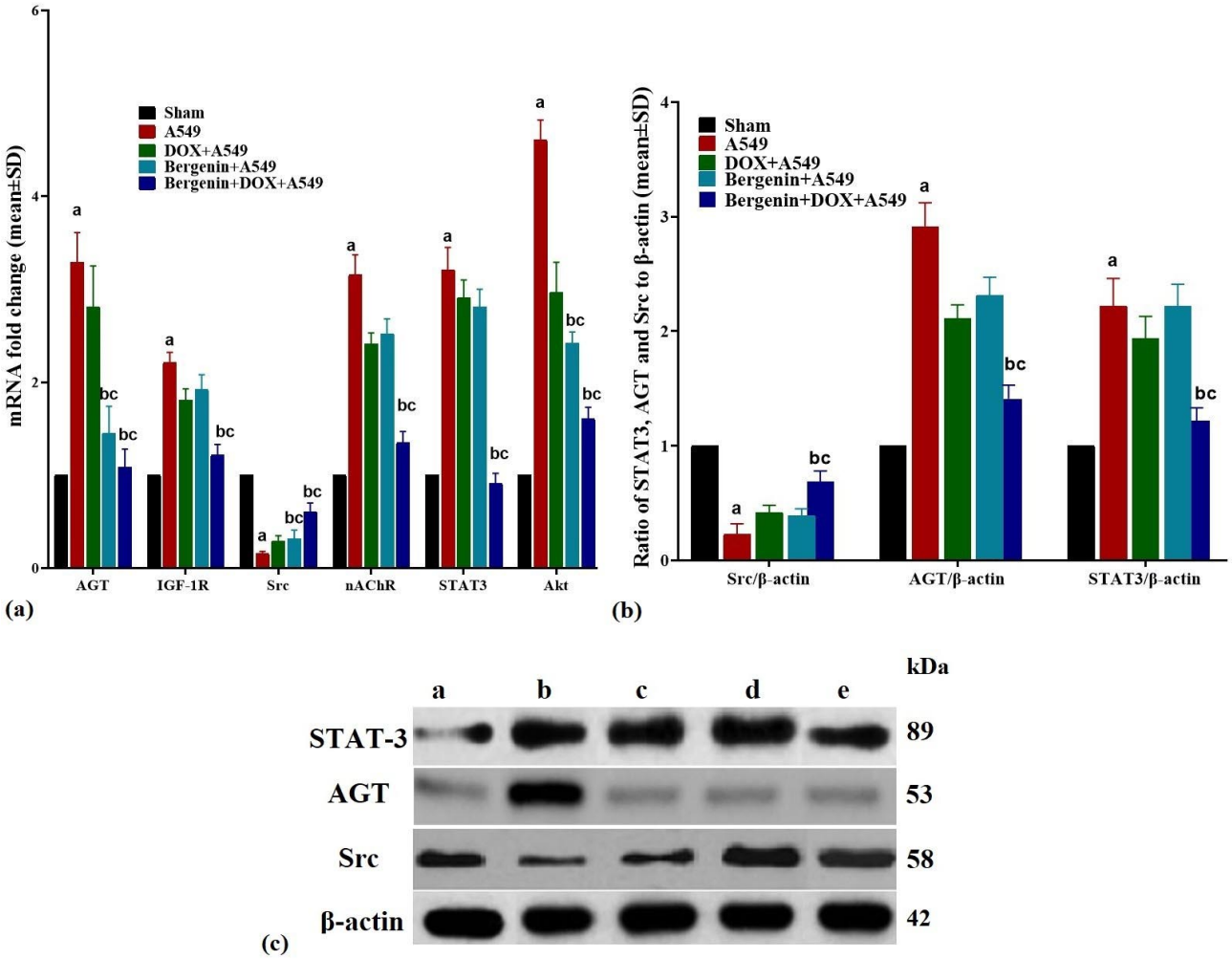

Fig. 4. (a) The mean lung tissue genes expression of AGT, IGF-1R, Src, nAChR, STAT3, Akt; (b) and (c) The mean tumor tissue protein expression of AGT, Src, and STAT3 in sham (a), A549 (b), DOX+ A549 (c), Bergenin + A549 (d), and Bergenin + DOX + A549 (e) groups. Statistical annotations: $^{a}(p < 0.05)$ Sham *vs.* A549; $^{b}(p < 0.05)$ Bergenin-treated groups *vs.* A549; $^{c}(p < 0.05)$ Bergenin+DOX+A549 *vs.* A549.

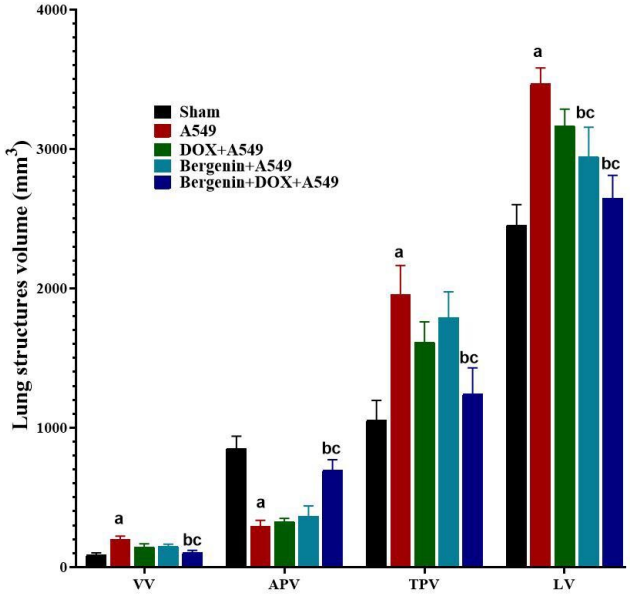

Fig. 5. Mean serum levels of stereological parameters in lung tissue in the different experimental groups. Lung volume (LV), tissue parenchyma volume (TPV), air parenchyma volume (APV), and vessels volume (VV). [a]($p < 0.05$) Sham *vs.* A549; [b]($p < 0.05$) Bergenin-treated groups *vs.* A549; [c]($p<0.05$) Bergenin+DOX+A549 *vs.* A549.

Lung tissues stereology

Mean values for lung volume (LV), tissue parenchyma volume (TPV), air parenchyma volume (APV), and vessels volume (VV) were measured in each experimental group (units as appropriate from your methods). Compared with Sham controls, the A549 group showed marked alterations in stereological parameters, indicating substantial structural changes associated with tumor presence. DOX treatment in the DOX+A549 groups partially modulated these parameters, while Bergenin-containing regimens (Bergenin+A549 and Bergenin+DOX+A549) produced further adjustments toward values closer to Sham (Figs. 5 and 6).

Lung tissues histopathology

Histopathological analysis was performed on lung tissues using hematoxylin and eosin staining. Within 10 days after injection, A549 cells were detected in multiple organs, including the lungs, indicating early metastasis. In lungs from the A549-treated mice, clusters of tumor cells were found nearthe main airways and throughout the alveolar tissue, accompanied by alveolar collapse (atelectasis) and lymphocyte infiltration. The lung parenchyma also exhibited hyperemia and edema. Doxorubicin (DOX) markedly reduced tumor cell accumulation by suppressing metastasis, but lymphocytic infiltration, alveolar atelectasis, and hyperemia persisted. In the Bergenin plus DOX group (Bergenin+DOX+A549), no tumor cell aggregates were detected; the alveolar spaces appeared normal, with no atelectasis or edema observed (Fig. 6).

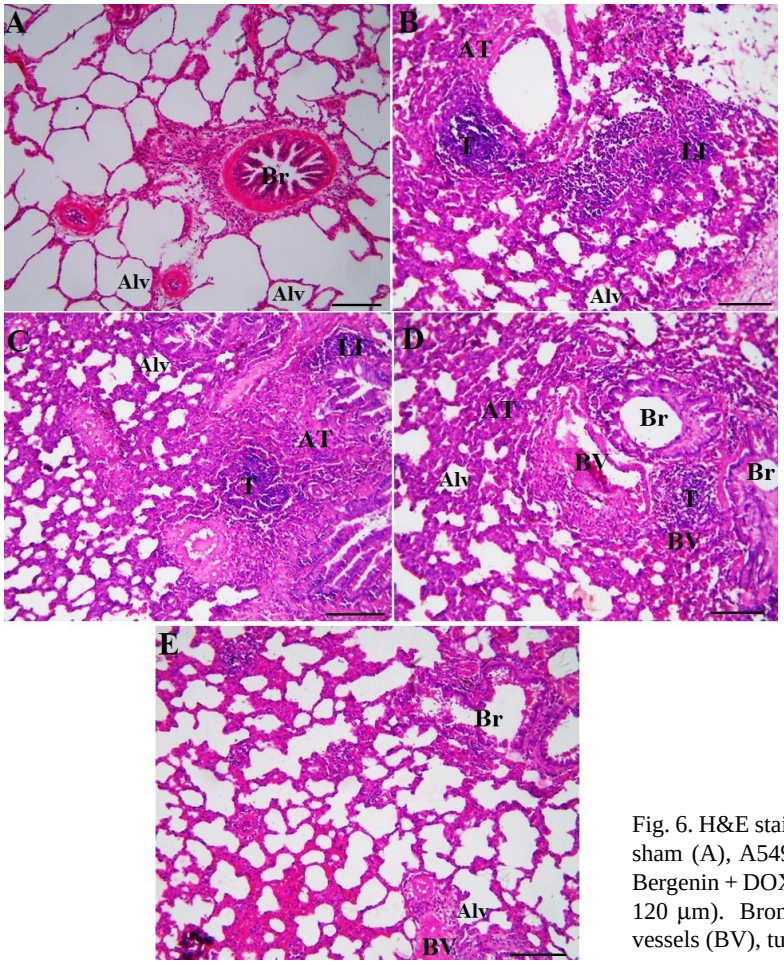

Fig. 6. H&E staining from lung tissues along with lungs isolated from sham (A), A549 (B), DOX+ A549 (C), Bergenin + A549 (D), and Bergenin + DOX + A549 (E) groups (H&E staining × 100, Scale bar = 120 μm). Bronchiole (Br), alveolus (Alv), atelectasis (AT), blood vessels (BV), tumor (T), and lymphatic infiltration (LI).

IHC assay results for AGT expression in tumor tissue.

Immunohistochemical analysis quantified AGT expression as percentages of positive cells (or relative optical density, depending on your method) across experimental groups. Compared with Sham controls, the A549 group showed marked increases in both AGT expression. Bergenin-containing regimens (Bergenin+A549 and Bergenin+DOX+A549) tended to reduce AGT expression relative to A549, with the Bergenin+DOX+A549 group often showing the greatest suppression (Fig. 7).

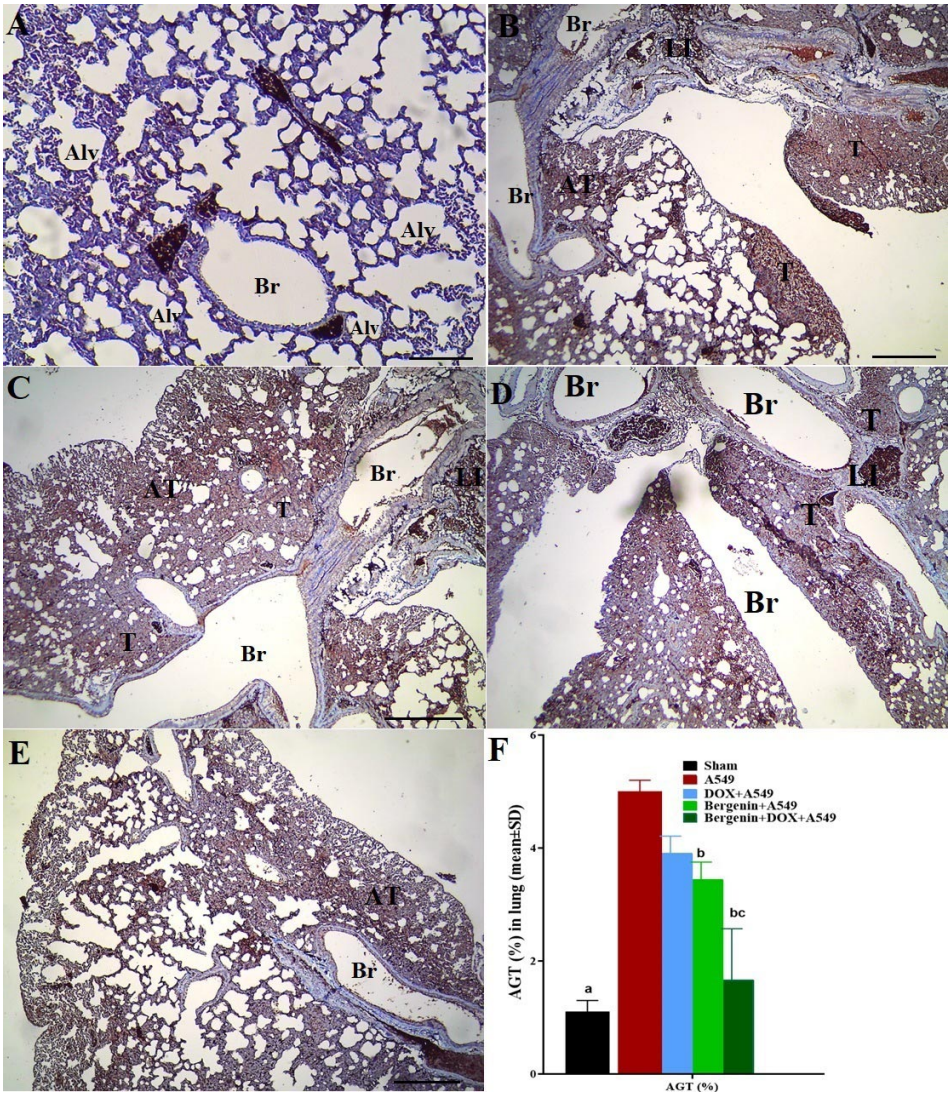

Fig. 7. IHC staining for AGT in sham (A), A549 (B), DOX+A549 (C), and Bergenin +A549 (D), Bergenin +DOX+A549 (E) groups (scale bar = 30 μm, ×400). a ($p < 0.05$) Sham *vs*. A549; b ($p < 0.05$) Bergenin-treated groups vs. A549; c ($p < 0.05$) Bergenin+DOX+A549 *vs*. A549. bronchiole (Br), alveolus (Alv), atelectasis (AT), tumor (T), and lymphatic infiltration (LI).

DISCUSSION

The investigation into Bergenin's effects on NNK-induced pulmonary cancer has provided valuable insights regarding its potential as a therapeutic agent for non-small cell lung cancer (NSCLC). Lung cancer remains a leading cause of cancer-related deaths worldwide, with NSCLC constituting approximately 85 % of all cases. The intricate biological behavior of NSCLC, coupled with its resistance to conventional therapies, underscores the need for innovative treatment strategies (Alduais *et al.*, 2023). Bergenin, a bioactive compound sourced from various

plants, has demonstrated promise due to its diverse mechanisms that target essential signaling pathways involved in tumor progression. In our study, we employed a mouse xenograft model to assess the anticancer effects of Bergenin on A549 cells, a commonly utilized NSCLC cell line. The results indicated that Bergenin not only inhibited tumor growth but also influenced various biochemical markers related to oxidative stress and inflammation. These findings are particularly significant considering the established role of the renin-angiotensin (RA) system in lung cancer development, although mechanistic insights into Bergenin's interactions with these pathways have been limited. The renin-angiotensin system has been implicated in promoting tumor growth and metastasis through several mechanisms, including the activation of inflammatory pathways and the enhancement of angiogenesis (Zhang *et al*., 2021). Our biochemical analyses revealed that Bergenin treatment resulted in a notable reduction in inflammatory mediators such as IL-6, TNF-α, IL-8, Ang II, and IFN-γ. This reduction is critical as it suggests that Bergenin may alleviate the inflammatory microenvironment that often supports tumor growth. By targeting these inflammatory cytokines, Bergenin appears to create a less conducive environment for tumor progression, thereby enhancing its overall therapeutic efficacy.

A pivotal aspect of our findings is the modulation of the nAChR/Src/STAT3 signaling pathway. Nicotinic acetylcholine receptors (nAChRs) play a crucial role in lung cancer biology, particularly in driving pro-proliferative signaling cascades (Xiong *et al*., 2023). Activation of the a7-nAChR by nicotine can trigger the activation of Src family kinases, which subsequently propagate signals to downstream effectors such as STAT3 (Arunrungvichian *et al*., 2023). In our study, Bergenin significantly downregulated the expression of phosphorylated STAT3, indicating its potential to inhibit the transcription of anti-apoptotic and pro-proliferative genes. This is particularly important as STAT3 is known to upregulate genes that promote cell survival and resistance to therapy, including members of the BCL-2 family and Cyclin D1 (Xu *et al*., 2018). By inhibiting this pathway, Bergenin may enhance the sensitivity of NSCLC cells to apoptosis, thereby decreasing tumor cell viability. Moreover, our study also examined Bergenin's influence on IGF-1R signaling, another critical pathway associated with tumor growth and survival. IGF-1R has been recognized for its role in supporting cellular proliferation and survival, especially in the context of cancer (Cao *et al*., 2020). The observed downregulation of IGF-1R expression following Bergenin treatment supports the idea that Bergenin may disrupt the signaling cascade that fosters tumor growth. This disruption is significant as it suggests that Bergenin can impair the signaling networks contributing to therapeutic resistance, particularly when used alongside conventional chemotherapeutic agents like doxorubicin. The synergistic effects of Bergenin when combined with doxorubicin were particularly noteworthy in our study. Doxorubicin is a widely used chemotherapeutic agent, yet its effectiveness can be compromised by various factors, including drug resistance and adverse side effects. Our findings indicate that Bergenin not only enhances the therapeutic efficacy of doxorubicin but also alleviates some of its associated toxicities. The combination treatment resulted in a more pronounced reduction in tumor growth and improved survival outcomes in the mouse xenograft model. This synergistic interaction suggests that Bergenin may act as a sensitizer, amplifying the effects of doxorubicin while potentially lowering the required dosage of the chemotherapeutic agent, thereby minimizing adverse effects. Additionally, our biochemical assessments of oxidative stress markers showed that Bergenin treatment led to increased activity of key antioxidant enzymes such as SOD, CAT, and GPx. The elevation of these antioxidant enzymes indicates that Bergenin may exert protective effects against oxidative damage, which is often exacerbated in cancer (Zhang *et al*., 2021). The reduction in lipid peroxidation and the increase in total thiol levels further support the notion that Bergenin helps maintain cellular redox balance, which is vital for normal cellular function and survival. Histopathological evaluations of tumor tissues provided further validation of Bergenin's anticancer effects. The immunohistochemical analysis revealed a significant reduction in the expression of AGT in tumor tissuesfollowing Bergenin treatment. This reduction aligns with our molecular findings, where real-time PCR demonstrated decreased expression of key oncogenes associated with tumor progression. The histological examination also indicated improvements in lung tissue architecture, suggesting that Bergenin may have protective effects on surrounding healthy tissues during cancer treatment. The implications of these findings extend beyond the laboratory setting, emphasizing the potential clinical relevance of Bergenin as a therapeutic agent in NSCLC. Given its traditional use and relatively favorable safety profile, Bergenin could serve as a valuable adjunct to existing treatment regimens, particularly for patients who exhibit resistance to standard therapies. Bergenin's ability to target multiple signaling pathways involved in tumor progression and inflammation positions it as a promising candidate for further clinical investigation.

It appears that polyphenolic compounds and other substances in Bergenin may protect normal parenchymal cells and inhibit the angiogenesis and metastasis of tumor

cells by reducing ROS levels, a hypothesis that warrants further investigation. Furthermore, research indicates that cancer cells have evolved mechanisms to cope with ROS, significantly overexpressing genes encoding SOD, CAT, and GPx. The term multidrug resistance (MDR) refers to the ability of many tumor cells to resist one or more chemotherapy drugs through these and other mechanisms. Doxorubicin, while widely used in certain tumors like breast and lung cancers, has its application limited due to the MDR phenomenon (Gote *et al*., 2021). Today, combination therapies are recommended to overcome the limitations of doxorubicin, enhancing its antitumor properties while also bolstering the immune system and protecting other organs from oxidative damage induced by its metabolites. Numerous studies have validated the potent antioxidant properties of Bergenin. For instance, Alanazi (2025) investigated the protective effects of Bergenin against carbon tetrachloride-induced hepatotoxicity in rats, finding that Bergenin increased the activity of ROS-reducing enzymes like CAT, SOD, and GPx, thereby lowering serum NO levels and tissue malondialdehyde (MDA) levels (Alanazi *et al*., 2025). Similarly, Alanazi *et al*. (2024), demonstrated that Bergenin, by enhancing SOD and GPx activity, mitigated oxidative damage induced by cadmium in rats (Alanazi *et al*., 2024). IL-6 and TNF-α are pro-inflammatory cytokines produced and secreted by various cell types, including tumor cells. They play a crucial role in the proliferation and differentiation of tumor cells and are typically found at elevated levels in serum and tumor tissues, particularly in lung tumors. Research indicates that high serum levels of IL-6 and IL-8 in animal models of NSCLC can weaken the effectiveness of doxorubicin treatment. Increased IL-6 levels are directly associated with tumor growth and metastasis; patients with elevated circulating IL-6 generally have a poorer prognosis and shorter survival times, while lower IL-6 levels correlate with better treatment responses (Chen *et al*., 2020).

The IL-6/JAK/STAT3 pathway regulates several genes involved in the proliferation, survival, and metastasis of lung cancer cells. IL-6-induced activation of JAK-STAT3 and NF-κB signaling promotes the translocation of STAT3 and NF-κB into the nucleus, leading to the expression of anti-apoptotic genes (e.g., Bcl-2, Bcl-xL, Mcl-1, survivin) (Johnson *et al*., 2018). The growth-promoting effects of IL-6 in tumor cells are mediated through several signaling pathways, including Ras/Raf/MEK/MAPK, PI3K/AKT, and STAT3/FOXM1/ATG7. Conversely, the roles of IL-8 and TNF-a in tumor invasion, progression, and metastasis are well established. High levels of IL-8 and TNF-α in NSCLCs correlate with increased invasiveness, and IL-8 also influences the expression of cell adhesion molecules such as E-cadherin and fibronectin in human lung cancer cells (Du, Wang & Zhang, 2025). Additionally, IL-8 and TNF-α enhance the expression of b3 integrin, further increasing the invasive potential of lung cancer cells through the activation of the STAT3/FOXM1/ATG7 pathway and, subsequently, NF-κB. NF-κB plays a critical role in inducing IL-8 gene transcription via several mediators, including LPS, TNF-α, and oxidative stress (Wu *et al*., 2023). The IL-8/PI3K/Akt/NF-κB/β3 integrin axis is considered one of the most important therapeutic targets for inhibiting the growth of metastatic lung tumors. As discussed regarding ROS and lung tumor growth, ROS stimulate IL-8 secretion, activating the Erk signaling pathway, which subsequently promotes the migration of NSCLCs. Therefore, suppressing IL-8 and the associated pathways, which contribute to angiogenesis and tumorigenesis, could be therapeutically valuable in inhibiting the invasion and metastasis of lung tumors (Li, 2024). It appears that the compounds in Bergenin achieve this by modulating these pathways and influencing the expression of cell adhesion molecules (β3 integrin, fibronectin, and E-cadherin) as well as the secretion of angiogenic factors like VEGF, warranting further exploration.

CONCLUSION

In conclusion, the findings from our study underscore the significant potential of Bergenin as a therapeutic agent against NSCLC. By targeting critical signaling pathways such as nAChR/Src/STAT3 and IGF-1R, Bergenin demonstrates a multifaceted approach to inhibiting tumor growth and enhancing chemosensitivity. The synergistic effects observed when combined with doxorubicin further highlight its promise as a complementary strategy in lung cancer therapy. As we continue to unravel the complexities of lung cancer signaling networks, Bergenin stands out as a candidate worthy of further exploration in clinical settings. The need for innovative therapeutic strategies in the fight against lung cancer is urgent, and Bergenin may play a crucial role in addressing this challenge.

Conflict of interest. The authors declared no potential conflicts of interest with respect to the research, authorship, and/or publication of this article.

Statement of Informed Consent and Ethical Approval. This study followed ethical standards for the use of animal subjects, ensuring that animal welfare was prioritized by minimizing any pain, discomfort, or distress. Ethical approval was obtained from the Wuhan Third Hospital, Tongren Hospital of WuHan University, Wuhan Hubei, China for conducting the animal research.

CHENG, Q.; YANG, T. & CHEN, C. Acción anticancerígena de la Bergenina en el cáncer pulmonar inducido por NNK: Mecanismos que involucran la activación del sistema renina-angiotensina por nAChR/Src/STAT3 y la señalización del IGF-1R. *Int. J. Morphol., 44(3)*:934-948, 2026.

RESUMEN: El sistema renina-angiotensina (AR) se ha relacionado con el desarrollo del cáncer de pulmón, pero aún se desconocen en detalle sus mecanismos. Se evaluaron los efectos de la Bergenina, un compuesto medicinal tradicional con propiedades antitumorales demostradas, sobre el cáncer de pulmón de células no pequeñas (CPCNP) mediante un modelo de xenoinjerto en ratones. Cincuenta ratones atímicos desnudos se dividieron en cinco grupos: un grupo control, un grupo con CPCNP sin tratamiento, un grupo tratado con doxorrubicina (DOX), un grupo tratado con Bergenina y un grupo con una combinación de bergenina y DOX. Bergenina se administró por vía oral a 50 mg/kg/día, mientras que DOX se administró por vía intraperitoneal a 50 mg/kg los días 10, 20 y 30. El crecimiento tumoral se monitorizó midiendo el tamaño, el volumen y el peso, y la supervivencia se analizó con estimaciones de Kaplan-Meier. Las evaluaciones bioquímicas e histopatológicas mostraron que Bergenina moduló los marcadores de estrés oxidativo, atenuó los mediadores inflamatorios (IL-6, TNF-α, IL-8, Ang II, IFN-γ) e impidió la progresión tumoral. El tratamiento redujo la expresión de vías de señalización asociadas con la supervivencia, proliferación y metástasis de las células tumorales, incluyendo nAChR/Src/STAT3 e IGF-1R. El análisis inmunohistoquímico demostró una expresión reducida de AGT, consistente con una menor proliferación de células tumorales. Las investigaciones moleculares respaldaron la influencia de Bergenina en vías críticas de apoptosis y angiogénesis. En combinación con DOX, Bergenina amplificó la eficacia terapéutica, lo que indica una posible interacción sinérgica. Nuestros resultados sugieren que la Bergenina podría ser un agente terapéutico que actúa sobre las cascadas de señalización relacionadas con nAChR/Src/STAT3 e IGF-1R/Akt en el cáncer de pulmón de células no pequeñas (CPCNP), lo que representa una estrategia complementaria prometedora a la quimioterapia estándar.

PALABRAS CLAVE: Bergenina; nAChR/Src/STAT3; Doxorrubicina; Cáncer de pulmón; Células A549.

REFERENCES

Akbaribazm, M.; Khazaei, M. R.; Khazaei, F.; & Khazaei, M. Doxorubicin and Trifolium pratense L. (Red clover) extract synergistically inhibits brain and lung metastases in 4T1 tumor-bearing BALB/c mice. *Food Sci. Nutr., 8(10)*:5557-70, 2020.

Alanazi, S. T.; Harisa, G. I.; & Salama, S. A. Modulating SIRT1, Nrf2, and NF-kB signaling pathways by bergenin ameliorates the cadmium-induced nephrotoxicity in rats. *Chem Biol Interact., 387*:110797, 2024.

Alanazi, S. T., Salama, S. A., Althobaiti, M. M., Alotaibi, R. A., AlAbdullatif, A. A., Musa, A. & Harisa, G. I. Alleviation of Copper-Induced Hepatotoxicity by Bergenin: Diminution of Oxidative Stress, Inflammation, and Apoptosis via Targeting SIRT1/FOXO3a/NF-kB Axes and p38 MAPK Signaling. *Biol. Trace Elem. Res., 203(6)*:3195-3207, 2025.

Alduais, Y.; Zhang, H.; Fan, F.; Chen, J.; & Chen, B. Non-small cell lung cancer (NSCLC): A review of risk factors, diagnosis, and treatment. *Medicine, 102(8)*:e32899, 2023.

Boo, H. J., Min, H. Y., Hwang, S. J., Lee, H. J., Lee, J. W., Oh, S. R., Park, C. S., Park, J. S., Lee, Y. M., & Lee, H. Y. The tobacco-specific carcinogen NNK induces pulmonary tumorigenesis via nAChR/Src/STAT3-mediated activation of the renin-angiotensin system and IGF-1R signaling. *Exp. Mol. Med., 55(6)*:1131-44, 2023.

Cao, D.; Lei, Y.; Ye, Z.; Zhao, L.; Wang, H.; Zhang, J.; He, F.; Huang, L.; Shi, D.; Liu, Q.; Ni, N.; Pakvasa, M.; Wagstaff, W.; Zhao, X.; Fu, K.; Tucker, A.B.; Chen, C.; Reid, R.R.; Haydon, R.C.; Luu, H.H.; He, T.C. & Liao, Z. Blockade of IGF/IGF-1R Signaling Axis with Soluble IGF-1R Mutants Suppresses the Cell Proliferation and Tumor Growth of Human Osteosarcoma. *Am. J. Cancer Res., 10*:3248-66, 2020.

Chen, M.; Chen, C.; Gao, Y.; Li, D.; Huang, D.; Chen, Z.; Zhao, X.; Huang, Q.; Wu, D.; Lai, T.; Su, G.; Wu, B. & Zhou, B. Bergenin-Activated SIRT1 Inhibits TNF-a-Induced Proinflammatory Response by Blocking the NF-kB Signaling Pathway. *Pulm. Pharmacol. Ther., 62*:101921, 2020.

Cuellar-Rufino, S.; Arroyo-Xochihua, O.; Salazar-Luna, A.; & Arroyo-Helguera, O. Iodine induces toxicity against Candida albicans and Candida glabrata through oxidative stress. *Iranian J. Microbiol., 14(2)*:260, 2022.

Dai, L.; Hu, J.; Yang, Y.; Qian, B.; & Zuo, X. 1p-Enh-regulated CYP4B1 alleviates NNK-induced heart failure and lung cancer via the STAT3 pathway. *Plos One, 20(9)*:e0331471, 2025.

Du, T.; Wang, W. & Zhang, R. Royal Jelly and Doxorubicin Suppressed Tumor Cells in the Xenograft Model of Lung Cancer via the STAT3/FOXM1/ATG7 Signaling Pathways in Athymic Nude Mice: A Biochemical, Immunohistochemically and Molecular Approach. *Toxicol. Res., 14(2)*:tfaf042, 2025.

Ekinci Akdemir, F. N.; Yildirim, S.; Kandemir, F. M.; Küçükler, S.; Eraslan, E. & Güler, M. C. Protective Effects of Baicalein and Bergenin Against Gentamicin-Induced Hepatic and Renal Injuries in Rats: An Immunohistochemical and Biochemical Study. *Basic Clin. Pharmacol. Toxicol., 136(1)*:e14121, 2025.

Faraji, M. H.; Akbaribazm, M.; Khazaei, M.; Niromand, E. & Khazaei, M. R. Synergistic Inhibitory Effects of Trifolium pratense L. Extract and Doxorubicin on 4T1 Tumor-Bearing Mice Are Mediated via Targeting the Wnt/b-Catenin Pathway and Reversal of Epithelial-Mesenchymal Transition. *Avicenna J. Phytomed., 15(5)*:1546, 2025.

Gote, V.; Nookala, A. R.; Bolla, P.K. & Pal, D. Drug Resistance in Metastatic Breast Cancer: Tumor Targeted Nanomedicine to the Rescue. *Int. J. Mol. Sci., 22(9)*:4673, 2021.

Horiguchi, M.; Yoshihara, K.; Watanabe, K.; Tsurudome, Y.; Mizukami, Y. & Ushijima, K. Circadian Rhythms of Clock Genes After Transplantation of Mesenchymal Stem Cells with Type 2 Diabetes Mellitus. *Int. J. Mol. Sci., 25(23)*:13145, 2024.

Islam, I˙.; Karagöz, A.; Aytug, H.; Bulduk, I. & Çoban, F. K. Apoptotic and Antiangiogenic Effects of Noscapine in Human Lung Cancer (A549) Cells. *Celal Bayar Üniv. Saglık Bilim. Enst. Derg., 9(1)*:42-49, 2022.

Johnson, D. E.; O'Keefe, R.A. & Grandis, J.R. Targeting the IL-6/JAK/STAT3 Signalling Axis in Cancer. *Nat. Rev. Clin. Oncol., 15(4)*:234-48, 2018.

Ju Hwang, C.; Choi, D. Y.; Park, M.H. & Hong, J. T. NF-kB as a Key Mediator of Brain Inflammation in Alzheimer's Disease. *CNS Neurol. Disord. Drug Targets, 18(1)*:3-10, 2019.

Kumar, P.; Ansari, K.; Srivastava, V.; Joseph, A. M.; Parmar, N. & Jhala, D. Bergenin Synergistically Enhances the Efficacy of Cisplatin and 5-FU: Strategy to Enhance Chemotherapy in Breast and Colorectal Cancer—An *In Vitro* Study. *Pharm. Sci., 31(4)*:452-63, 2025.

Li, J. Bee pollen and doxorubicin by synergistic effects inhibit the proliferation of breast tumors in 4T1 tumor-bearing BALB/c mice: A biochemical, immunohistochemical, and molecular approach. *Pharmacogn. Mag., 20(1)*:159-78, 2024.

Ma, T.; Hu, Y.; Guo, Y. & Zhang, Q. Human umbilical vein endothelial cells-derived microRNA-203-containing extracellular vesicles alleviate non-small-cell lung cancer progression through modulating the DTL/p21 axis. *Cancer Gene Ther., 29(1)*:87-100, 2022.

Mohana, A. A.; Roddick, F.; Maniam, S.; Gao, L. & Pramanik, B. K. Component analysis of fat, oil and grease in wastewater: Challenges and opportunities. *Anal. Methods, 15(39)*:5112-28, 2023.

Nikzad, M. B.; Sardar, M. A.; Aghababaeian, A.; Azimi, S. A.; Shafiee, M. & Abbasian, S. Inhibitory effect of swimming exercise and black seed nanocapsules on the expression of gene signal transducer and activator of transcription-3 on the lungs of Wistar rats exposed to nicotine-derived nitrosamine ketone (NNK). *Int. J. Cancer Manag., 18(1)*:e163669, 2025.

Pandey, P.; Lakhanpal, S.; Mahmood, D.; Kang, H. N.; Kim, B.; Kang, S.; Choi, J.; Moon, S.; Pandey, S.; Ballal, S.; Kumar, S.; Khan, F. & Kim, B. Bergenin, a bioactive flavonoid: Advancements in the prospects of anticancer mechanism, pharmacokinetics and nanoformulations. *Front. Pharmacol., 15*:1481587, 2025.

Patel, S.; Fridovich-Keil, S.; Rasmussen, S. A. & Fridovich-Keil, J. L. DAB-quant: An open-source digital system for quantifying immunohistochemical staining with 3,3'-diaminobenzidine (DAB). *PLoS One, 17(7)*:e0271593, 2022.

Pearl, M. H.; Zhang, Q.; Palma Diaz, M. F.; Grotts, J.; Rossetti, M.; Elashoff, D.; Gjertson, D. W.; Weng, P.; Reed, E. F. & Tsai Chambers, E. Angiotensin II type 1 receptor antibodies are associated with inflammatory cytokines and poor clinical outcomes in pediatric kidney transplantation. *Kidney Int., 93(1)*:260-69, 2018.

Salminen, A.; Kaarniranta, K. & Kauppinen, A. Insulin/IGF-1 signaling promotes immunosuppression via the STAT3 pathway: Impact on the aging process and age-related diseases. *Inflamm. Res., 70(10)*:1043-61, 2021.

Tekin, S. & Seven, E. Assessment of serum catalase, reduced glutathione, and superoxide dismutase activities and malondialdehyde levels in keratoconus patients. *Eye, 36(10)*:2062-6, 2022.

Vasilescu, D. M.; Phillion, A. B.; Kinose, D.; Verleden, S. E.; Vanaudenaerde, B. M.; Verleden, G. M.; Van Raemdonck, D.; Stevenson, C. S.; Hague, C. J.; Han, M. K.; Cooper, J. D.; Hackett, T. L. & Hogg, J. C. Comprehensive stereological assessment of the human lung using multiresolution computed tomography. *J. Appl. Physiol., 128(6)*:1604-16, 2020.

Wu, L.; Li, J.; Liu, T.; Li, S.; Feng, J.; Yu, Q.; Zhang, J.; Chen, J.; Zhou, Y.; Ji, J.; Chen, K.; Mao, Y.; Wang, F.; Dai, W.; Fan, X.; Wu, J. & Guo, C. Quercetin shows anti-tumor effect in hepatocellular carcinoma LM3 cells by abrogating JAK2/STAT3 signaling pathway. *Cancer Med., 8(10)*:4806-20, 2019.

Wu, Y.; Xu, M.; Feng, Z.; Wu, H.; Wu, J.; Ha, X.; Wu, Y.; Chen, S.; Xu, F.; Wen, H.; Li, S. & Wu, X. AUF1-induced circular RNA hsa_circ_0010467 promotes platinum resistance of ovarian cancer through miR-637/LIF/STAT3 axis. *Cell. Mol. Life Sci., 80(9)*:256, 2023.

Xiong, R.; Du, Y.; Chen, S.; Liu, T.; Ding, X.; Zhou, J.; Wang, Z. & Yang, Q. Hypermethylation of the ADIRF promoter regulates its expression level and is involved in NNK-induced malignant transformation of lung bronchial epithelial cells. *Arch. Toxicol., 97(12)*:3243-58, 2023.

Xu, N. W.; Chen, Y.; Liu, W. E.; Chen, Y. J.; Fan, Z. M.; Liu, M. & Li, L. J. Inhibition of JAK2/STAT3 signaling pathway suppresses proliferation of Burkitt's lymphoma Raji cells via cell cycle progression, apoptosis, and oxidative stress by modulating HSP70. *Med. Sci. Monit., 24*:6255-65, 2018.

Zhang, G.; Wang, H.; Zhang, Q.; Zhao, Z.; Zhu, W. & Zuo, X. Bergenin alleviates H2O2-induced oxidative stress and apoptosis in nucleus pulposus cells: Involvement of the PPAR-g/NF-kB pathway. *Environ. Toxicol., 36(12)*:2541-50, 2021.

Zhang, H. F.; Gao, X.; Wang, X.; Chen, X.; Huang, Y.; Wang, L. & Xu, Z. W. The mechanisms of renin-angiotensin system in hepatocellular carcinoma: From the perspective of liver fibrosis, HCC cell proliferation, metastasis and angiogenesis, and corresponding protection measures. *Biomed. Pharmacother., 141*:111868, 2021.

Corresponding author:
Dr. Conghua Chen
Department of Thoracic Surgery
Yangxin County People's Hospital
Huangshi
Hubei, 435200
CHINA

E-mail: chench202609@outlook.com

ORCID ID: 0009-0008-3583-276X